INFN Istituto Nazionale di Fisica Nucleare

ISTITUTO NAZIONALE DI FISICA NUCLEARE

Laboratori Nazionali di Frascati

INFN-12-24/LNF
18th December 2012

Beam dynamics studies and design of the LINAC-LER transfer line for the electron Injector of SuperB

S. Guiducci, D. Pellegrini

Abstract

The transfer line from the Linac to the Low Energy Ring (LER) for the latest layout of the SuperB project is a critical part of the injector. It must implement a total of 149_ small-radius bending in the horizontal plane, a vertical dogleg and a final vertical angle to match the tilt of the LER. Details of the design are explained in this note together with the beam dynamics studies and the estimation of the maximum acceptable energy error for an efficient injection.

*Published by **SIDS–Pubblicazioni***
Laboratori Nazionali di Frascati

CONTENTS

OVERVIEW

This technical note is intended to be an integration and an extension of the master thesis: "Beam dynamics studies and optimization of the SuperB Injection System", by Dario Pellegrini, 2012. In that work the injector of SuperB was studied. It was composed by the transfer line from the Dampin Ring (DR), the Bunch Compressor (BC), the Main Linac and a straight matching section to the Injection Cell of the Low Energy Ring (LER). The bunch compressor was optimized in order to reduce the final energy spread of both electron and positron beam. The effects of misalignments of the Linac quadrupoles and cavities were studied and an effective correction scheme was proposed. The collective effects like Coherent Synchrotron Radiation and Wakefields were evaluated and proved to be small on the low-charge-long bunches of the SuperB injector.

Since that time, the radius of the Damping Ring has been increased to better fit the magnets and its energy was raised from 1.0 GeV to 1.1 GeV to keep a low damping time. New parameters of the beam extracted from the Damping Ring were calculated and needed to be tracked along the injector up to the main rings.

The attention here is focused on the electron beam which is the critical one due to the lower adiabatic damping in the Linac and the small bending radius of the transfer line from the Linac to the LER. In the first part of this note, the injector will be presented and its parts described with emphasis on the modifications made to the set up illustrated in the thesis. Then we will focus on the design of the transfer line explaining its critical points and characterizing it. Finally the results of the beam dynamics studies on the whole electron injector will be presented.

Note that this is not the definitive layout of the injector as the geometry still need to be adjusted, but includes all the features that influence the parameters of the beam.

1 THE SUPERB INJECTOR

The SuperB injection system delivers full energy, low emittance beams to the main rings: 4.2 GeV electrons for the Low Energy Ring (LER) and 6.7 GeV positrons for the high Energy Ring (HER). The injection has been designed to be continuous in order to keep nearly constant beam current and luminosity. Fig. 1.1 illustrates the footprint of the machine fitted in the construction site at the Cabibbo Lab, Tor Vergata, Rome, Italy.

The injector is displaced tangentially to the rings. Once extracted from the DR (visible in the bottom-right corner of Fig. 1.1), the positrons travel in an almost straight line to the HER, while the electrons must accomplish a nearly U turn to be injected in the LER after the acceleration in the Linac.

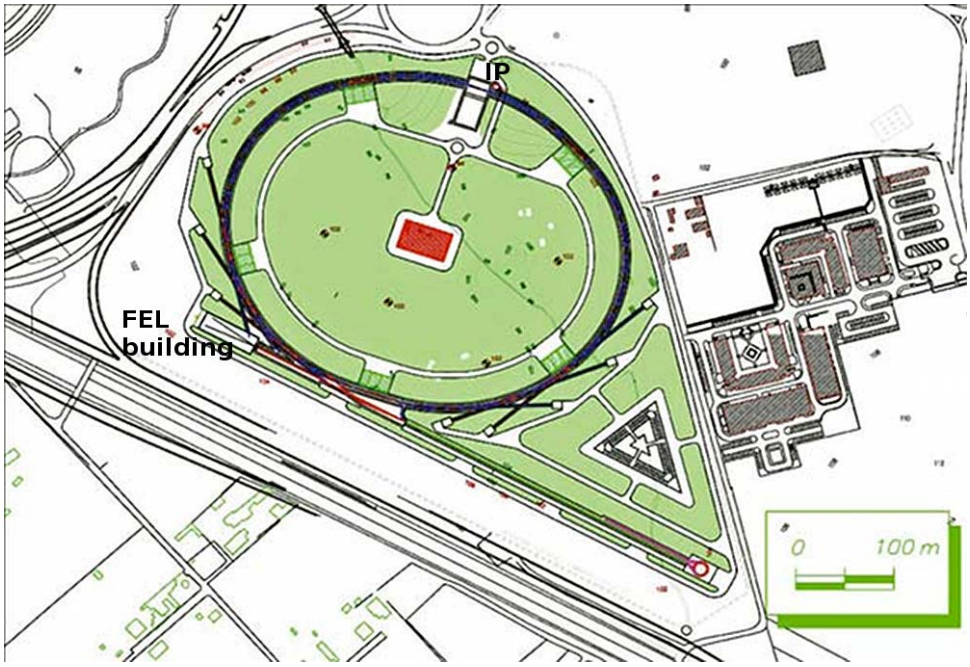

Figure 1.1. *The present layout of SuperB at the Cabibbo Lab, Tor Vergata, Rome, Italy.*

The bunch extracted from the Damping Ring has a 6D gaussian shape whose parameters are summarized in Tab. 1.1.

Parameter	Symbol	Unit	Electron	Positron
Energy	E	GeV	1.1	1.1
Horizontal emittance	ε_x	nm	30.4	
Vertical emittance	ε_y	nm	1.1	
Bunch length (RMS)	σ_s	mm	4.8	4.8
Momentum spread (RMS)	δ	‰	0.678	0.678
Horizontal optical function	β_x	m	4.13	4.13
Horizontal optical function	α_x	-	0.258	0.258
Vertical optical function	β_y	m	2.20	2.20
Vertical optical function	α_y	-	0.640	0.640
Number of particles	N_b	-	$1.87 \cdot 10^9$	$1.87 \cdot 10^9$
Total charge	C	pC	−300	300

Table 1.1. *Parameters of the beam extracted from the new Damping Ring.*

After the extraction the bunches travel the injector whose lattice is presented in Fig. 1.2. First of all a transfer line aligns the extracted bunches to the Linac and matches the optical functions. Just before entering the Linac the bunches travel the compressor which reduces their length to a value suitable to be accelerated by the S-band RF. At the end of the Linac the electrons are extracted by a pulsed magnet. The transfer line to the LER must accomplish a total of 149° horizontal bend plus a 0.90 m vertical shift exiting with a small-but-non-zero vertical angle to compensate the tilt of the rings.

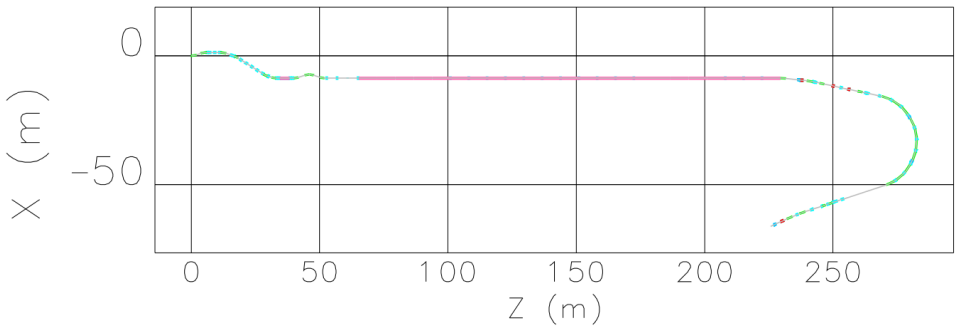

Figure 1.2. *Lattice scheme of the electron injector from the exit of the DR to the end of the LER injection cell.*

1.1 BUNCH COMPRESSOR

The bunch compressor is composed by an RF-cavity working on the zero crossing which introduces a momentum spread correlated with the longitudinal position along the bunch. A chicane then provides the longitudinal compression according to the longer distance travelled by the lower energy particles with respect to the higher energy ones.

In principle a bunch compressor could reduce the bunch length to an arbitrary value. This however requires to use a very high voltage of the cavity thus resulting in a high final energy spread, according to the conservation of the phase-space volume. The energy spread is one of the critical parameter of the SuperB injection and it must be minimized at the end of the Linac, tuning the bunch compressor to the best compromise between the induced energy spread and the length reduction.

This was made for the thesis work, finding the best set up to be shared by both electron and positron beams. However the new Damping Ring parameters require a new optimization. For the moment the compressor has been adjusted changing only the cavity voltage to minimize the final energy spread of the electron beam. Small improvements in the beam quality may be obtained acting also on the R_{56} of the chicane.

The CSR effects in the magnets of the chicane were kept, however they have been proven to be negligible as they affect $\Delta p/p$ at the 10^{-7} order of magnitude.

1.2 LINAC

The Linac keeps the same number of cavity (46) and the same FODO cell structure as described in the thesis. The voltage of the cavities has been slightly reduced in order to exit at 4.18 GeV with the entering energy raised from 1.0 GeV to 1.1 GeV.

Errors on the alignment were not taken into account at this step as it was shown that they can easily be compensated, even in presence of wakefields, with a very small emittance increase.

The wakefields were turned off due to the fact that the bunches are longer than the provided definition of the Green function. This results in differences at the order of 10^{-5} $\Delta p/p$. Previously they were partially

compensated by advancing the Linac phase from 90° to 89° thus, with them turned off, the phase have been taken back to 90°.

The energy error has been provided with small variations of the total voltage of the Linac. All fields of the downstream magnets have been kept fixed.

2 DESIGN OF LINAC-LER TRANSFER LINE

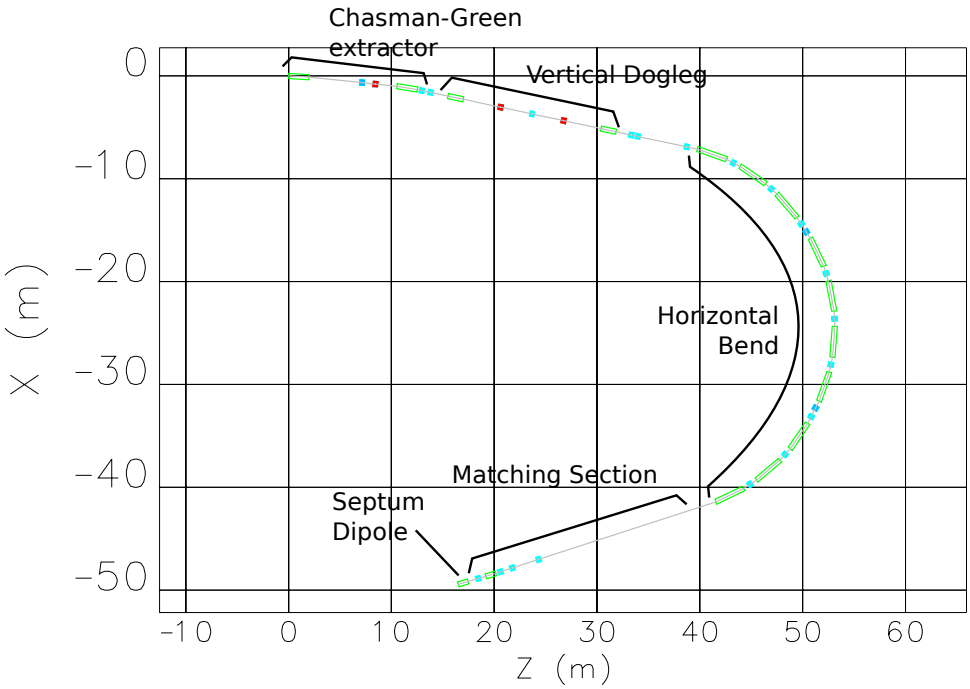

Figure 2.1. *Lattice scheme of the Linac-LER Transfer line. Travelling through the line, the beam encounters: the extractor, the vertical dogleg, the horizontal bending, the final matching section and the septum magnet of the LER injection cell.*

The transfer line must provide a total horizontal bending of 149°, a vertical gap of 0.9 m and a final small vertical angle of about 2.5 mrad to match the tilt of the LER. The electron beam is extracted from the Linac with a pulsed dipole, while the injection in the LER is operated with a septum magnet.

The dipoles used in the bending section are 3 m long, sector magnets with a maximum field of 1.2 T, therefore providing a 15° bending with a radius of 12 m.

The maximum field gradient used in the quadrupoles is 23 T/m, the same of the ones used in Damping Ring. The length of the quadrupoles has been arbitrary fixed at 0.35 m.

At the exit of the Linac the emittance of the beam is quite small while a significant momentum spread is still present, so the beam envelop is mainly driven by the dispersion and the effect of the optical functions is low. Therefore, when operating on the lattice of the transfer line particular care must be taken in order to contain the dispersion, while the optical functions can be raised up to 300 m without evident consequences.

Fig. 2.1 presents the lattice of the transfer line, whose parts are explained in the next sections.

2.1 EXTRACTION

The extraction of the electron beam from the Linac is provided by a pulsed magnet whose switching time must be lower than 10 ms, it has been assumed a maximum of 6° kick. Few meters of drift space are necessary to obtain the required separation from the Linac.

The extraction is done in the horizontal plane. A doublet and a dipole are used to correct the dispersion. The optical functions in the Linac have been kept constant. To keep them under control in the extractor, a QD has been introduced immediately after the Chasman-Green QF as shown in Fig. 2.2 where the optical functions and the horizontal dispersion are shown.

2.2 VERTICAL DOGLEG

The current design implements the vertical dogleg right after the extraction. It consists in an achromatic beam translation which uses two equal QDs to focus the vertical dispersion between the two opposite bending dipoles. To control the optical functions a QF has been placed in the middle being transparent to the dispersion. The vertical dispersion is plotted in Fig. 2.3

The dogleg has been implemented using 3.6° bending dipoles therefore resulting 16 m long. The defocusing quadrupoles are already at their maximum value. Length reduction can be achieved, if necessary, using longer or stronger quadrupoles and so being able to increase the dipole bending.

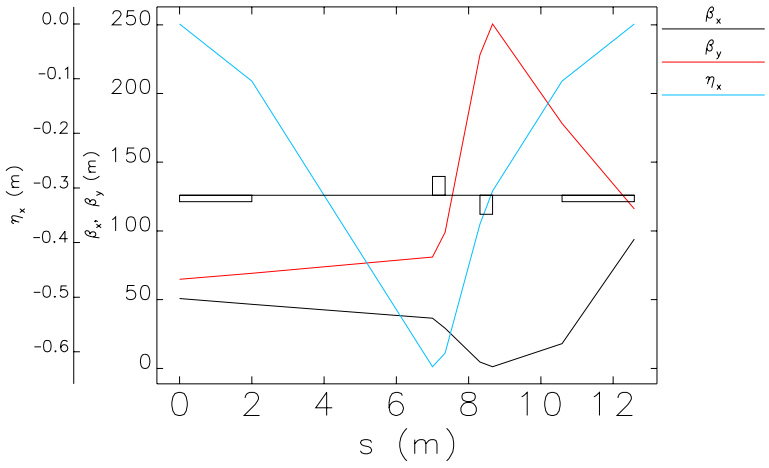

Figure 2.2. *Plot of the optical functions and of the dispersion in the modified-Chasman-Green extractor. The sign of the dispersion is negative as the bend is opposite to the one of the LER.*

The dogleg can easily be moved before or after the bending section and, with some worldly wisdom necessary to avoid conflicts with the Linac elements, it may also be used to extract the beam. The vertical angle is small enough to be introduced at the beginning of the line. The induced vertical shift at the end of the line can be compensated acting on the dogleg length or strength.

2.3 BENDING SECTION

The bending section is the critical part of the transfer line. The dispersion generated by the dipoles sums up along the U-turn resulting in a quite big $R_{56} = \int_{s_i}^{s_f} D(s)/\rho(s) ds$ which, together with the initial energy spread, causes the lengthening of the bunch. Two ways have been explored in order to provide a design: the regular FODO and the inverted dispersion.

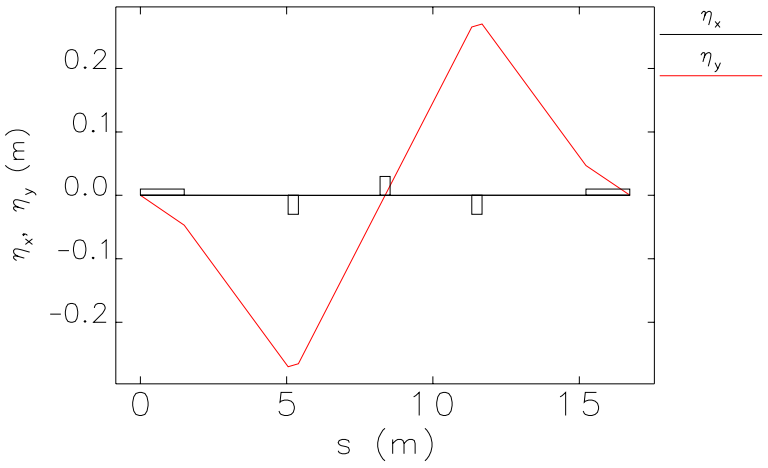

Figure 2.3. *Plot of the dispersion in the vertical dogleg.*

2.3.1 Regular FODO

The regular FODO is the first attempt to provide a lattice for the bending section. It is a regular pattern of 4 FODO cells, each of them hosting 2 bending dipoles, for a total of 8. At the beginning of the section an extra dipole is used together with a quadrupole to raise the horizontal dispersion to the periodic value and match the optical functions. The same pattern is implemented at the end of the bending section. A drift space of 1.5 m is kept between the dipoles to host the quadrupoles, this can be reduced in next designs. The lattice and the optical functions are shown in Fig. 2.4.

The advantages of the regular FODO are that it can easily be adjusted and it has moderate quadrupole strengths. However the resulting R_{56} is about 3 m and the bunch length is increased by a factor 10, becoming similar to the one of the stored beam. The dispersion and the R_{56} can be contained reducing the length of the dipoles without increasing the field and introducing more quadrupoles. However this results in more straight sections, so larger total radius, and cost increase.

2.3.2 Inverted Dispersion

In this lattice the quadrupoles are used to control the dispersion and to invert it at the centre of the section, therefore lowering the total

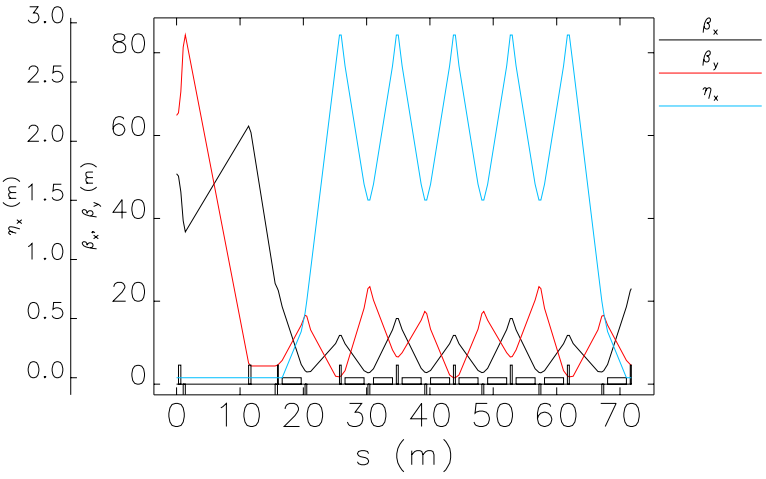

Figure 2.4. *Plot of the dispersion and of the optical functions in the regular fodo bending. The first quadrupoles match the optical functions, the first dipole and the following quadrupole adjust the dispersion to the periodic value. All the central quadrupoles share the same field.*

R_{56}. The idea consists in letting the dispersion raise in the first two dipoles with a QD in between. Then a QF easily focuses it. When the dispersion is near to the zero crossing a doublet is used to control the optical functions. In the middle of the cell α_x, α_y and D'_x are matched to zero. The second half of the section is the symmetric copy of the first half, so that at the end of the line the initial conditions are restored.

The technique to match this pattern is to work on half of the bending section, ignoring the optical functions first, and providing a good trend of the dispersion. Then acting on the doublet and on the initial values of the optical functions one can try to obtain a stable lattice. α_x and α_y have to be matched to zero at the centre of the cell and so also D', this can be achieved operating small variation also of the other quadrupole strengths.

The provided design comes with an R_{56} of just 0.8 m, resulting in just a doubling of the bunch length.

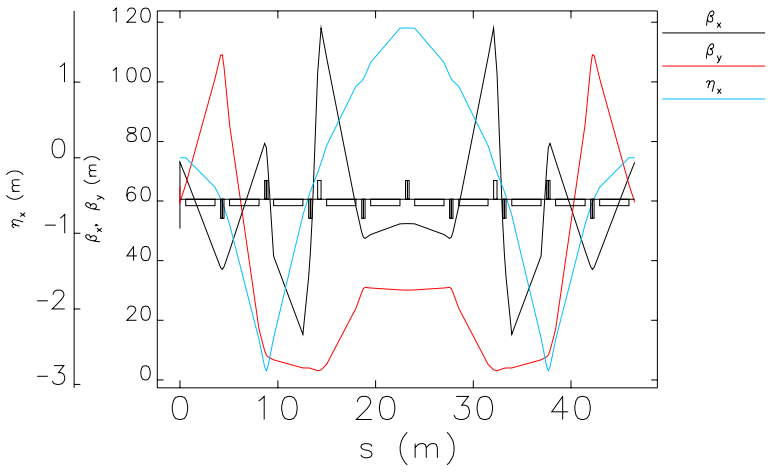

Figure 2.5. *Plot of the dispersion and of the optical functions in the inverted dispersion scheme. Note the QF which reverts the dispersion and the doublet placed near the inversion point.*

2.4 INJECTION

At the end of the transfer line, the optical functions have to be matched to the ring values. This is made in a matching section composed by a triplet of quadrupoles. A dipole magnet is used to raise the dispersion to the ring unperturbed value. Finally the septum dipole aligns the injected beam with the stored one, matching also the dispersion derivative. No care has been taken to avoid conflicts with the elements of the LER injection cell.

2.5 IRREGULAR FODO: AN ALTERNATIVE DESIGN

An attempt was made to combine the extraction and the bending section. The extractor dipole provide the initial dispersion which is then controlled in an irregular FODO. This results in a more compact design with fewer matching quadrupoles and the R_{56} can be slightly reduced with respect to the regular FODO case. Adopting this lattice the dogleg has to be placed after the bending section. Fig. 2.6 shows an example

of lattice and of the optical functions which can be obtained in a such design.

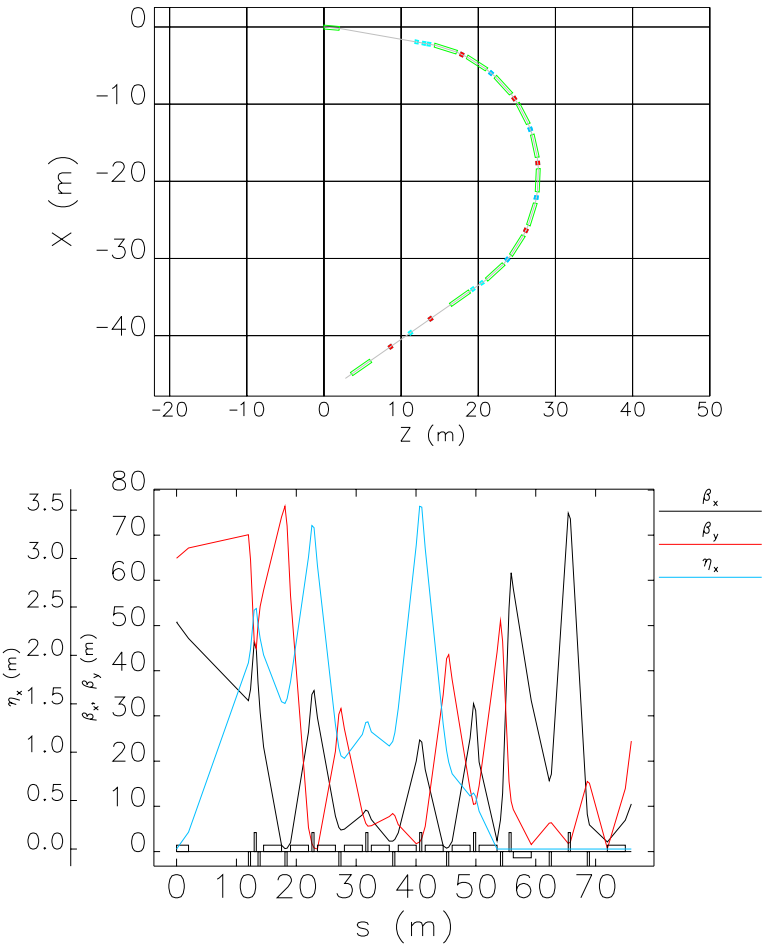

Figure 2.6. *Plot of the dispersion and of the optical functions in the irregular FODO scheme wich combines the extraction from the Linac with the horizontal bending. At the end of the line the vertical dogleg take place.*

3 BEAM DYNAMICS

Full tracking from the damping ring to the end of the LER injection cell has been done. The final beam distribution was analysed in conjunction with the acceptance of the LER.

For the bending section of the Linac-LER transfer line the lattice which provides the inversion of the dispersion has been studied. It is the most conservative for the beam length, however the effects of its strong irregular focusing on the final beam distribution need to be checked even in presence of an energy error.

To find the required acceptances for the injection, for each particle in the bunch the invariant was computed and the distribution was made. This distribution is often far from Gaussian, especially for the vertical phase space in which the bunch is centred on the origin, so a way to produce a consistent result is to find the interval which starts from zero and contains a fixed percentage (99.7 %) of the invariants distribution. The interval width is then expressed in term of the sigma of the stored bunch.

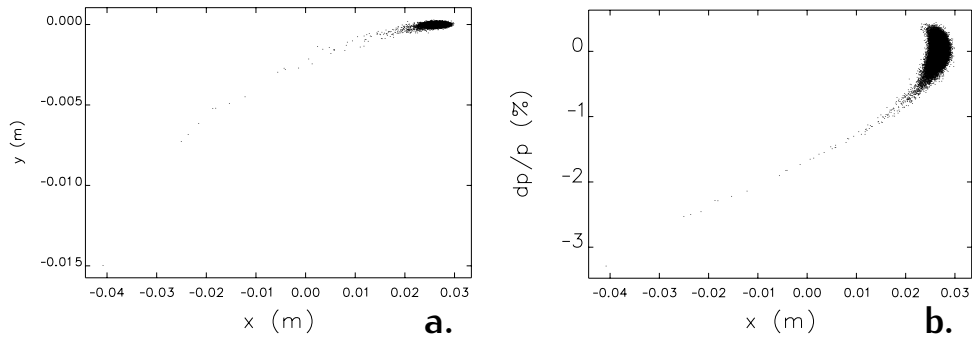

Figure 3.1. *a: x-y distribution of the bunch at septum. b: x-dp/p distribution of the bunch at septum.*

3.1 BEAM DYNAMICS IN THE TRANSFER LINE

Fig. 3.2 shows the envelopes and the optical functions for the full transfer line with the inverted dispersion bending section. You may notice that even if both the dispersion and the optical functions are low at the end of the line, the envelope of the beam is increased with respect to the beginning of the line. This is due to a tail that the bunch acquires during the bending which is shown in Fig. 3.1.a where the transverse slice after the inverted dispersion bending is presented. This tail comes from the chromaticity and non-linear terms and is composed mostly by the lower energy particles, however for a positive energy error, even the highest energy particles present a similar behaviour. The correlation between the final horizontal position and momentum spread is show in Fig. 3.1.b. For small energy deviations the tail include ~ 1.3 % of the total particles and it is lost against the septum. A reduction of these value may be obtained including few sextupoles in the transfer line in order to correct the chromaticity.

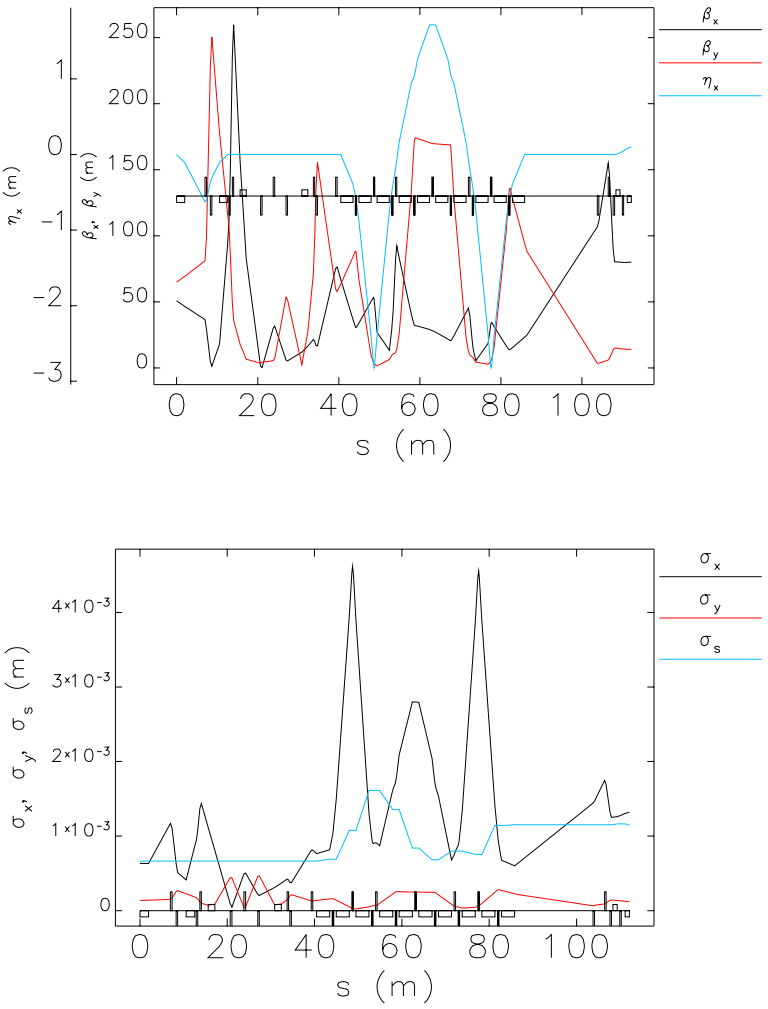

Figure 3.2. *Plot of the optical functions (top) and of the beam envelopes (bottom) along the full transfer line with the inverted dispersion bending section.*

3.2 HORIZONTAL TRANSVERSE DYNAMIC

The tracked size of the stored bunch at septum is: $\sigma_x^{sto} = 0.678$ mm therefore, to provide a $26\sigma = 17.6$ mm offset at septum (which is placed at 30σ) a kick of 0.183 mrad has been applied.

At the septum, the horizontal separation between the two bunches is:

$$\langle x_{inj} \rangle - \langle x_{sto} \rangle = 4\sigma_x^{sto} + D_s + 3\sigma_x^{inj}$$

where $D_s = 4$ mm indicates the septum thickness, and the tracked value of $3\sigma_x^{inj}$ is 0.874 mm.

A 3/2pi rotation in the phase space take place in the following part of the injection cell, so that at the end of it both of the bunches are centred, but the injected one keeps a non-null-average tilt which will be damped by the synchrotron radiation.

Fig. 3.3 presents the beam distributions at the septum and at the end of the cell for the nominal energy of the injected beam.

Fig. 3.4 shows the distribution of the horizontal Courant-Snyder invariant computed for the injected beam at the end of the injection cell. The required acceptance to embrace 99.7 % of that distribution corresponds to 17.8 σ_x^{sto}, recomputing the value considering 3σ from the centroid we obtain 17.3 σ_x^{sto}.

3.2.1 Energy Error

The effect of an error on the energy of the Linac has been investigated varying the acceleration in the linac while keeping constant the fields in the magnets of the transfer line.

The inverted dispersion bending has a non-linear response to the energy variations. At the end of the bending section, both high and low energy particles are driven closer the septum even if the dispersion is matched to zero there. To compensate for this, the offset of the injector with respect to the injection cell has been adjusted moving the whole injector. This ensures that losses at septum are always ~ 1.3 %. The two final correctors will be adjusted to provide the correct offset in the final part of the transfer line.

Tab. 3.1 collects the invariants and the offsets computed for different accelerations in the Linac. Fig. 3.5 presents as a sample the horizontal phase space at the septum for an energy error of -5 ‰.

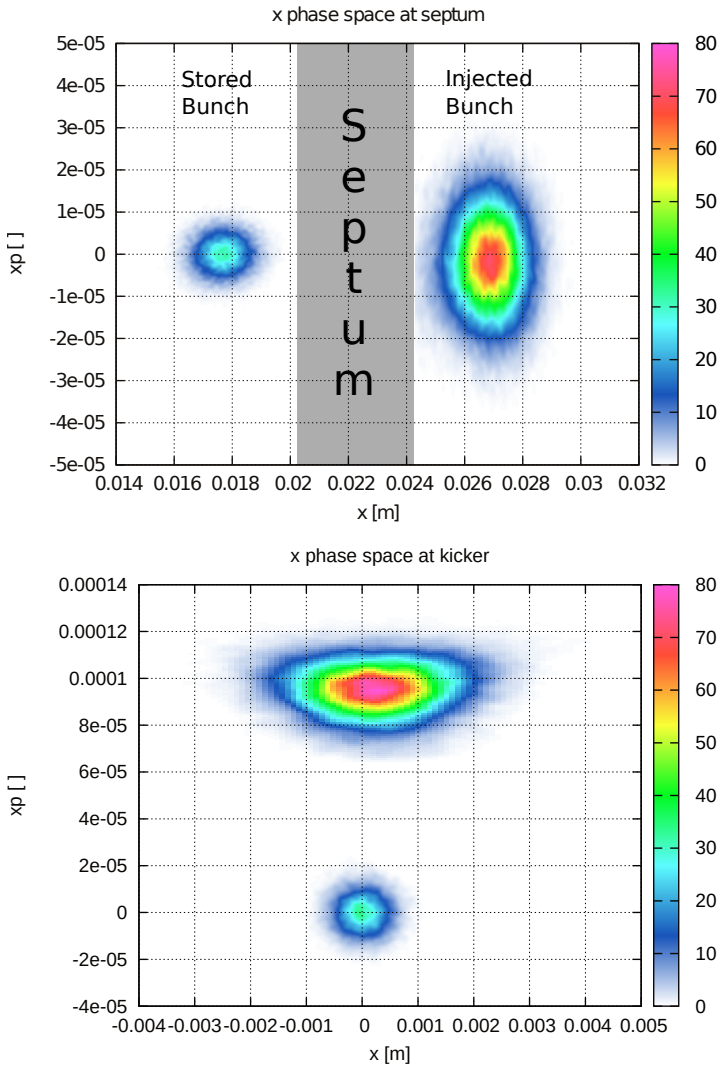

Figure 3.3. *Density plots for the horizontal phase space of both the stored and the injected electron bunches at septum (top) and at kicker (bottom).*

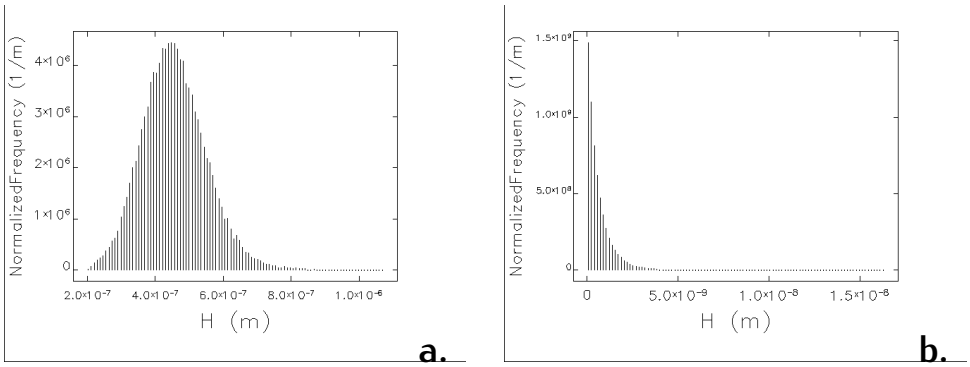

Figure 3.4. *Histograms of the distributions of the Courant-Snyder invariants for the injected bunch at the end of the injection cell. a: horizontal. b: vertical.*

energy offset	offset value	invariant 99.7%
5 ‰	34.1 mm	34.3 σ_x^{sto}
3 ‰	29.5 mm	23.9 σ_x^{sto}
1 ‰	27.4 mm	19.1 σ_x^{sto}
0 ‰	27.5 mm	17.8 σ_x^{sto}
−1 ‰	28.4 mm	19.6 σ_x^{sto}
−3 ‰	31.4 mm	23.0 σ_x^{sto}
−5 ‰	35.6 mm	27.5 σ_x^{sto}

Table 3.1. *Size of the horizontal invariant and offset values, for different final Linac energies. The offset are referred to the unperturbed stored orbit and ensures that losses are* ∼ 1.3 %.

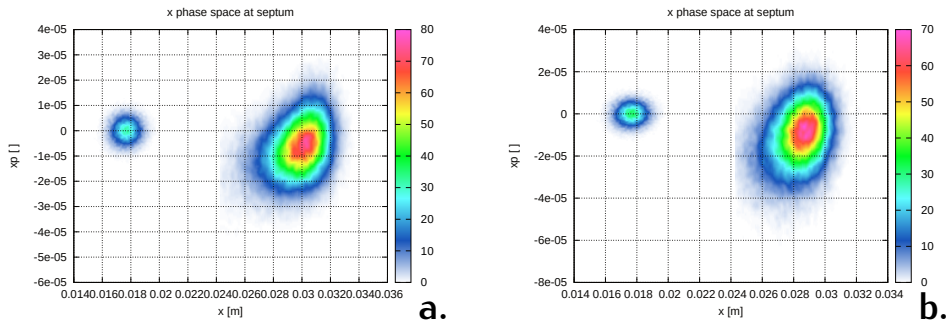

Figure 3.5. *Horizontal distribution of the injected beam with an energy error of a: −3 ‰ and b: 3 ‰ at the septum. The stored beam is also plotted.*

3.3 VERTICAL TRANSVERSE DYNAMIC

In the vertical dimension the injected bunch is centred and perfectly matched to the ring. Fig. 3.6 presents the vertical phase space of the injected bunch at the end of the injection cell. Fig. 3.4.b shows the distribution of the particles invariants. The 99.7 % of the particles are within 26.9 σ_y^{sto}.

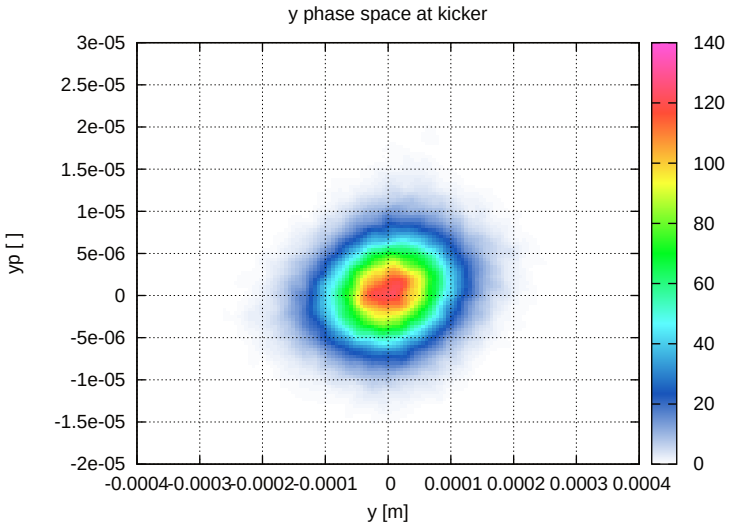

Figure 3.6. *Density plot for the vertical phase space of the injected electron bunches at kicker.*

3.3.1 Energy Error

The result of an energy error in the vertical phase space is the accentuation of the non-linearities. The bunch is deformed and becomes unmatched, however, as a consequence of the very small emittance, we do not expect losses coming from the vertical distribution. Fig. 3.9 presents the vertical phase space of the bunch at the kicker tracked with an energy error of $\pm 3‰$.

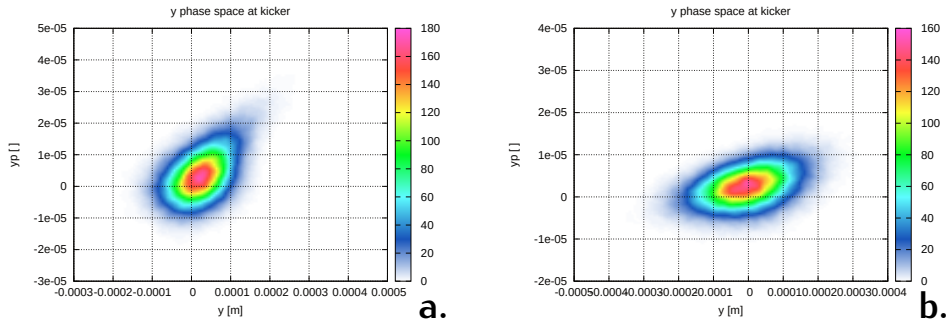

Figure 3.7. *Vertical distribution of the injected beam with an energy error of a: −3 ‰ and b: 3 ‰ at the kicker.*

3.4 LONGITUDINAL DYNAMICS

Fig. 3.8 presents the longitudinal distribution of the injected bunch, the RF invariants are superimposed. Note that the bunch travels from the right to the left. The correlation between longitudinal position and energy is due to the residual R_{56} of the horizontal bending with the inverted dispersion. The regular FODO produces a bunch which is 5 times longer. However from Fig. 3.8 it is clear that the critical parameter is not the bunch length, but the energy spread, which also causes the elongation of the injected bunch as it turns in the main ring.

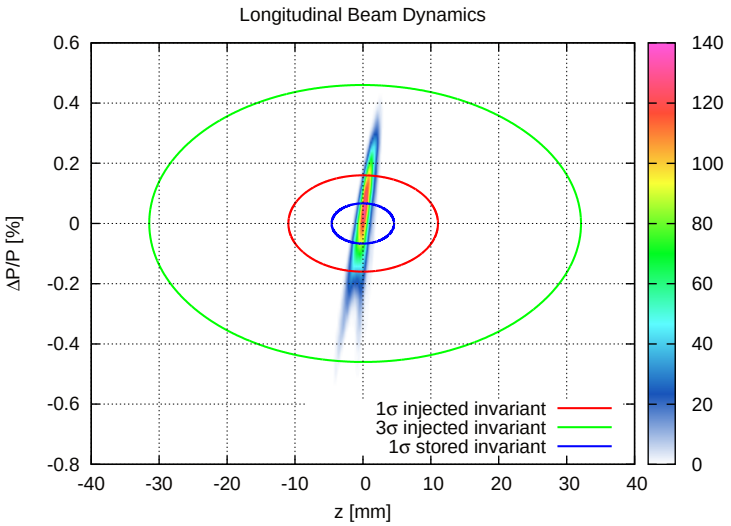

Figure 3.8. *Density plots for the longitudinal phase space of the injected electron bunches at kicker. RF invariants are superimposed. The travellind direction of the bunch is from right to left.*

3.4.1 Energy Error

In the longitudinal direction the bunch reacts linearly on energy variations. The bunch is shifted in the phase space according to the R_{56} of the bending section. Again the critical parameter is the acquired energy offset, while the longitudinal displacement has just a small variation.

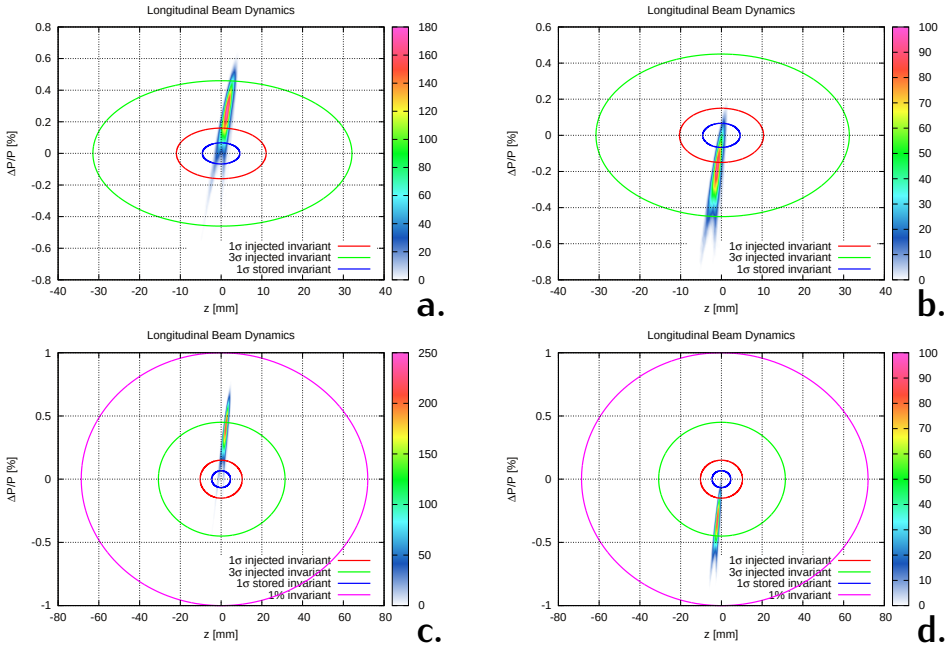

Figure 3.9. *Longitudinal distribution of injected bunches for different energy errors of the Linac voltage, a:* 3 ‰ *b:* −3 ‰ *c:* 5 ‰ *d:* −5 ‰*. The ellipses represent (from the smaller to the bigger)* 1σ *of the stored beam,* 1σ *of the centered injected beam,* 3σ *of the centered injected beam and* 1% *of* $\Delta p/p$.

Energy compressor

To better fit the injected bunch in the dynamic aperture of the ring an energy compressor may be setted up. It may take advantage of the position-energy correlation generated in the bending section and consist of just an RF-cavity placed after it. The performances of such a system may be studied in future as by now the existing energy spread is expected to be acceptable for an efficient injection.

4 CONCLUSIONS

4.1 TL MAGNETS TABLE

In the following tables the magnet parameters for the different sections of the transfer line are reported. It is easy to compute the magnetic field scaling the strength of the magnet as follows:

$$B_{dip}[T] = \frac{p[GeV/c]\ \theta[rad]}{0.3\ L[m]} \tag{4.1}$$

for the dipoles, and:

$$G_{quad}[T/m] = 3.34\ k\ p[GeV/c] \tag{4.2}$$

for the quadrupoles. In case of the electron injector of SuperB: $p = 4.18\ GeV$.

Chasman-Green Extractor

Quadrupoles	Length [m]	Strength
QFE	0.35	1.6
QDE	0.35	-1.2
Dipoles	Length [m]	Angle [mrad]
2×BHI	2	105

Vertical Dogleg

Quadrupoles	Length [m]	Strength
QFDL	0.35	1.6
2×QDDL	0.35	-1.6
Dipoles	Length [m]	Angle [mrad]
2×BHI	1.5	63

Horizontal Bending

Quadrupoles	Length [m]	Strength
2×QD1	0.35	-0.65
2×QF1	0.35	1.3
2×QD2	0.35	-0.63
2×QF2	0.35	1.5
2×QD3	0.35	-0.48
QF3	0.35	0.006
Dipoles	Length [m]	Angle [mrad]
10×BHI	3	262

Matching Sections

Quadrupoles	Length [m]	Strength
QFE-DL	0.35	1.6
QDE-DL	0.35	-0.96
QFDL-B1	0.35	1.1
QDDL-B	0.35	-1.6
QFDL-B2	0.35	0.54
QDB-MR1	0.35	-0.14
QFB-MR	0.35	0.88
QDB-MR2	0.35	-0.93
QDB-MR3	0.35	-0.008
Dipoles	Length [m]	Angle [mrad]
2×BHF	1	35

4.2 SUMMARY AND OUTLOOK

In this note the beam dynamics studies on the complete electron injector of SuperB have been presented, accorded to the new layout of the Damping Ring at 1.1 GeV and the proposed Linac-LER transfer line.

In the first chapter of the note the injector is described with particular attention to the modifications necessary to fit the new damping ring with respect to the one used for the thesis "Beam dynamics studies and optimization of the SuperB Injection System", by Dario Pellegrini, 2012.

In the second chapter the possibilities explored for the Linac-LER transfer line are presented and explained. To contain the bunch elongation a bending scheme which inverts the dispersion has been chosen.

The third chapter analyses the beam dynamics in the whole injector evaluating the effect of an energy error on the final 6D distribution of the injected beam. The maximum tolerance on the linac acceleration to allow an efficient injection is about 2 ‰. The total losses of the injected bunch is about 1.3 %, affecting mostly the low energy tails.

Future works consist in geometrical adjustments and tracking in the main rings to verify the stability and the damping of the injected bunch.